SCIENTIFIC REPORTS

OPEN

SUBJECT AREAS:
ELECTRONIC DEVICES
STRUCTURAL PROPERTIES
NANOSCALE MATERIALS

Received
16 July 2013

Accepted
3 February 2014

Published
27 February 2014

Correspondence and requests for materials should be addressed to M.G.L. (lagally@engr.wisc.edu)

* Current address: Materials Science Division, Argonne National Laboratory, Argonne, Illinois 60439 USA.

Nanomembrane-based materials for Group IV semiconductor quantum electronics

D. M. Paskiewicz[1]*, D. E. Savage[1], M. V. Holt[2], P. G. Evans[1] & M. G. Lagally[1]

[1]Department of Materials Science & Engineering, University of Wisconsin-Madison, Madison, Wisconsin 53706 USA, [2]Center for Nanoscale Materials, Argonne National Laboratory, Argonne, Illinois 60439 USA.

Strained-silicon/relaxed-silicon-germanium alloy (strained-Si/SiGe) heterostructures are the foundation of Group IV-element quantum electronics and quantum computation, but current materials quality limits the reliability and thus the achievable performance of devices. In comparison to conventional approaches, single-crystal SiGe nanomembranes are a promising alternative as substrates for the epitaxial growth of these heterostructures. Because the nanomembrane is truly a single crystal, in contrast to the conventional SiGe substrate made by compositionally grading SiGe grown on bulk Si, significant improvements in quantum electronic-device reliability may be expected with nanomembrane substrates. We compare lateral strain inhomogeneities and the local mosaic structure (crystalline tilt) in strained-Si/SiGe heterostructures that we grow on SiGe nanomembranes and on compositionally graded SiGe substrates, with micro-Raman mapping and nanodiffraction, respectively. Significant structural improvements are found using SiGe nanomembranes.

Strain breaks the crystallographic symmetry in materials, leading, among other effects, to changes in the electronic band structure[1]. In Si, strain engineering methods are used to tune the electronic properties (in particular charge carrier mobility) to enhance performance[2] in conventional devices (by now well established and commercially exploited), to create new devices, such as extremely fast flexible electronics[3], and to enable new research, for example, in Group IV quantum electronics[4]. In Ge, strain can change the band structure sufficiently to make it direct-band-gap, thus creating the prospect for Group IV optoelectronic and photonic devices integrated with Si-based electronic devices[5]. In complex metal oxides, as another example, strain can sensitively influence the ferroelectric state: the paraelectric-to-ferroelectric transition temperature can shift by hundreds of degrees with strain; the size, shape, and orientation of ferroelectric domains is altered depending on the magnitude and direction of applied strain[6]; and changes in crystalline symmetry due to strain can induce ferroelectric effects in materials that do not exhibit electric polarization in bulk form at any temperature[7].

In Group IV quantum electronics the ability to lift the degeneracy of the Si conduction band minimum with strain is particularly important. The formation of single-electron quantum devices in Si-based systems[8] requires a very thin layer of tensilely strained Si epitaxially grown and confined between SiGe layers. The Si layer is tensilely strained because the lattice constant of SiGe is larger than that of Si. A 2-dimensional electron gas (2DEG, also referred to as a Si quantum well [QW]) is created in the strained-Si layer and a series of lateral gates, when biased properly, confines single electrons (quantum bits or qubits). Long spin coherence times in Si make Si-based materials ideal for these quantum electronic devices[9].

The challenge in fabricating such quantum electronic devices is the lack of structural uniformity laterally in the strained-Si layer when fabricated in the conventional way, leading to electrostatic nonuniformities in the Si 2DEG and thus inconsistencies in the electronic behavior of qubits fabricated on different parts of the substrate. Whereas it has been known that the conventional method, described below, leads to these difficulties, an alternative method was not available until recently[10]. A quantitative comparison of the structural quality of the substrates fabricated by the old and the new methods, as well as the strained-Si QW layer grown on them, has been lacking. We provide this comparison here. We demonstrate that the local strain uniformity and mosaic structure of the strained-Si layer is highly dependent on the structural quality of the substrate used for this heteroepitaxial growth.

Conventionally, strained-Si QWs are epitaxially (pseudomorphically) grown on thick, compositionally graded, plastically strain relaxed (i.e., irreversible reduction in strain) SiGe films grown on Si substrates[11] (Figure 1a). Plastic strain relaxation occurs via a network of buried misfit dislocations (Figure 1a-iii.). A non-uniform

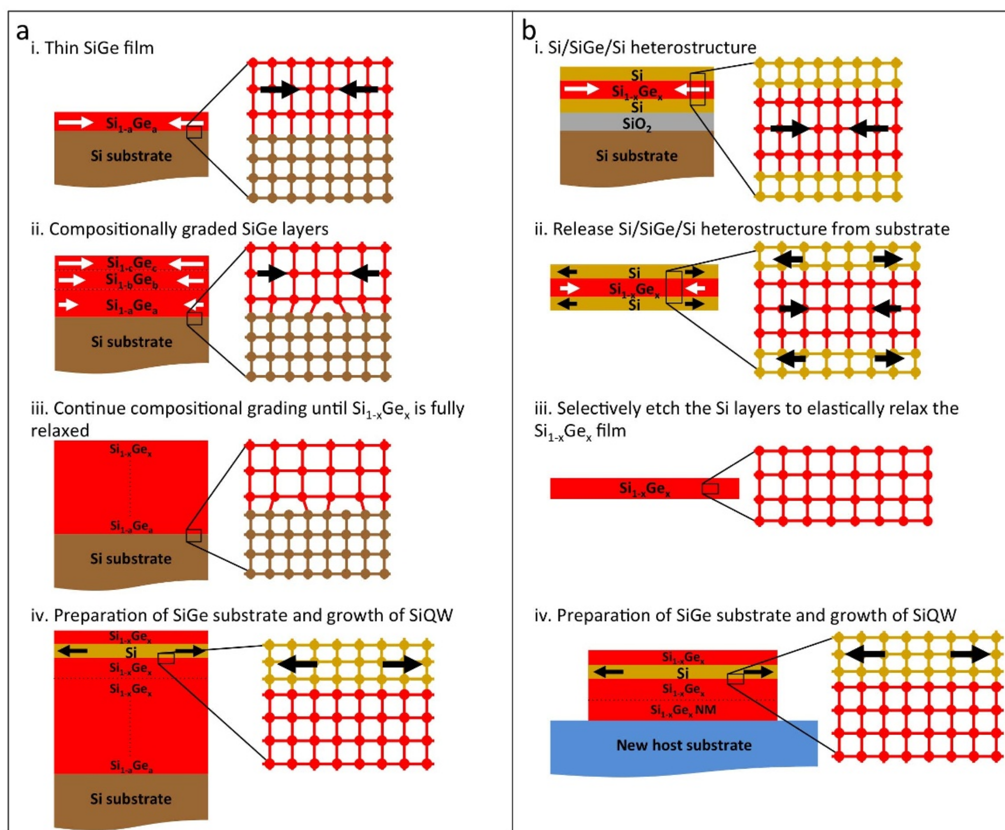

Figure 1 | Schematic diagrams of fabrication processes for conventional compositionally graded, plastically relaxed SiGe substrates and the new elastically relaxed SiGe NMs. (a) Conventional approach: i. The initial, low-Ge-composition $Si_{1-a}Ge_a$ is strained to the Si lattice constant. ii. As the total SiGe alloy thickness and Ge composition increases ($c > b > a$), the SiGe begins to relax via misfit dislocations. iii. The alloy composition can be step graded or continuously graded (typically ~10%/µm) until the desired Ge composition is reached and the alloy is fully relaxed. iv. The relaxed graded substrate is then chemically-mechanically polished before epitaxial growth of a constant-composition, lattice-matched $Si_{1-x}Ge_x$ buffer layer and the strained-Si QW. (b) New NM process: i. A thin $Si_{1-x}Ge_x$ layer is epitaxially grown on a silicon-on-insulator (SOI) substrate followed by a Si capping layer similar in thickness to the Si template layer of the SOI. The $Si_{1-x}Ge_x$ layer is strained to the Si lattice constant. ii. The trilayer Si/SiGe/Si heterostructure is released from the original Si substrate by selectively etching away the SiO_2 layer. The trilayer is allowed to strain share: some of the compressive strain in the SiGe layer is transferred as tensile strain to the outer Si layers. iii. The outer Si layers are selectively etched away. Removing the outer layers allows the $Si_{1-x}Ge_x$ NM to relax elastically to the bulk lattice constant appropriate for the alloy composition. iv. The SiGe NM is transferred to a new host substrate (in this work an oxidized Si wafer) and bonded there before a lattice matched SiGe buffer layer and strained-Si QW are epitaxially grown on top.

distribution of misfit dislocations in the compositionally graded, plastically relaxed SiGe substrate will result in a non-uniform strain distribution in the epitaxial strained-Si layer grown on top[12,13]. Additionally, the nature of the plastic relaxation results in crystallites that have small misorientations with respect to each other, called crystalline tilt or mosaic structure, in the SiGe substrate[14] that is also transferred to the strained-Si QW[15]. These structural imperfections can result in changes in the conduction band offsets between Si and SiGe (caused by strain variations) and charge carrier scattering from rough interfaces and crystalline imperfections (caused by mosaic structure); both effects contribute to the inconsistencies in the performance of quantum electronic devices described above.

The alternative to the conventional approach becomes possible via semiconductor nanomembrane synthesis, a relatively new area of research with a wide range of device applications[16,17]. This technology provides unstrained single-crystalline sheets of SiGe[10], on which strained-Si/relaxed SiGe heterostructures are grown. To fabricate these SiGe sheets, one grows a sandwich of Si/strained-SiGe/Si on SOI (Figure 1b-i.) and then releases it from the oxide (Figure 1b-ii.). The SiGe sheet is obtained by preferentially etching the Si layers from the Si/strained-SiGe/Si sandwich (Figures 1b-iii.). During this process, the strained single-crystal SiGe sheet relaxes elastically to the bulk lattice constant appropriate to the composition. The SiGe sheet is transferred to a host substrate and bonded there (Figure 1b-iv.). One can then grow thick, epitaxial, lattice-matched SiGe films on the SiGe NMs before growing the thin Si QW and SiGe capping layer required for the quantum electronic devices. Details for the fabrication of SiGe NM substrates and epitaxial growth on transferred SiGe NM substrates are described elsewhere[10].

Results and Discussion

Strain. We measure the strain variation in the heterostructures with micro-Raman spectroscopy. Figure 2a provides an example of a Raman spectrum from a 20 nm $Si_{0.73}Ge_{0.27}$/12 nm Si/~2 µm $Si_{0.73}Ge_{0.27}$ heterostructure (viewed from the top down) grown on a 45 nm $Si_{0.73}Ge_{0.27}$ NM, the latter being the transferred NM described above. The graph shows the Raman-active modes of the strained Si and the corresponding Si-Si bond of the alloy, along with the peak fitting function. Figures 2b and c show, respectively, maps of the Raman frequencies from the Si-Si bond in SiGe and in strained Si, over ~20 × 13 µm² areas of the heterostructure. The maximum frequency shift in both layers (Si and SiGe) over this area is slightly larger (±0.4 cm^{-1}) than the noise level (±0.3 cm^{-1}) of the instrument over the time frame in which this map was taken. A relative frequency shift of ±0.4 cm^{-1} from the average corresponds to a strain variation of ±0.05% in both the SiGe[18] and the Si layers[19]. If

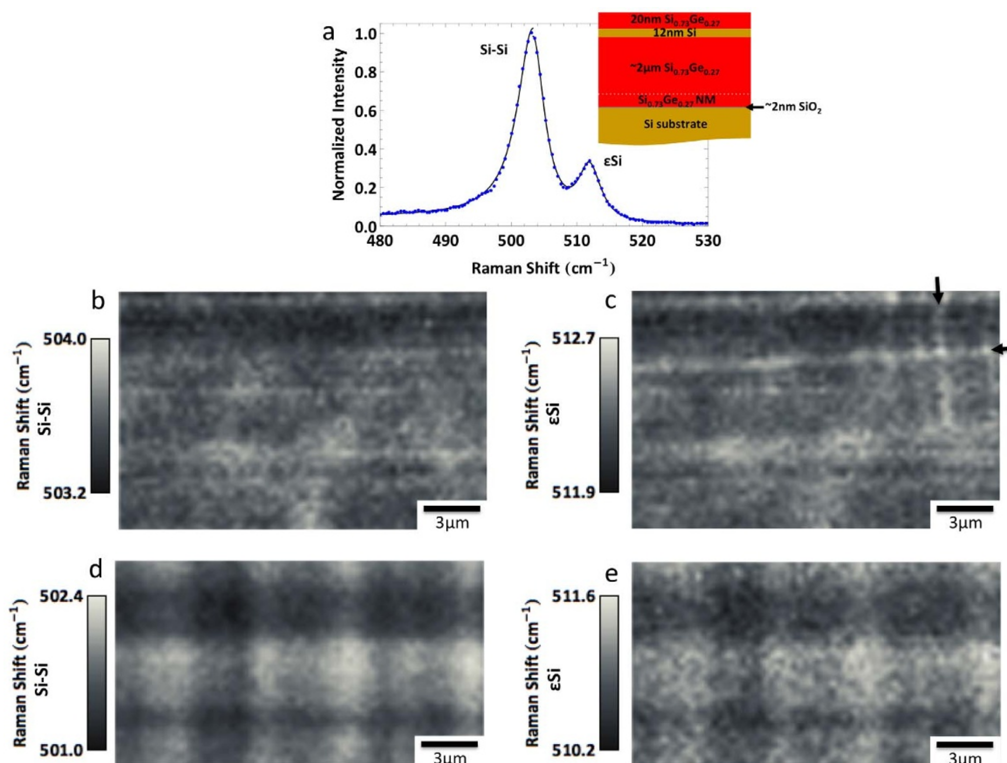

Figure 2 | Raman spectroscopy of a strained-Si layer grown on conventionally prepared graded and NM SiGe(001) substrates. (a) Raman spectrum from a 20 nm $Si_{0.73}Ge_{0.27}$/12 nm Si/~2 μm $Si_{0.73}Ge_{0.27}$ heterostructure grown on a (001) oriented 45 nm $Si_{0.73}Ge_{0.27}$ NM transferred and bonded to an oxidized Si wafer. The data (dotted) and fitting function (solid) are plotted; the peaks for the Si-Si bond in SiGe and in strained Si (εSi) are labeled. The intensity of the peaks is proportional to the amount of material being sampled; the strained-Si peak is less intense because the layer is much thinner (~12 nm) than the amount of SiGe being sampled (~70 nm for 442 nm wavelength laser source). (b–e) Micro-Raman maps of (b) the Si-Si mode and (c) the εSi mode corresponding to the spectrum in (a), and the (d) Si-Si mode and (e) εSi mode of the same 20 nm $Si_{0.71}Ge_{0.29}$/12 nm Si/~2 μm $Si_{0.71}Ge_{0.29}$ heterostructure grown instead on a commercially available polished graded $Si_{0.71}Ge_{0.29}$ substrate. Heterostructures grown on the latter clearly show large regular variations in strain reminiscent of crosshatch. We occasionally see small areas, such as that indicated by the arrows in (c) where the strained-Si layer grown on the NM substrate appears to show initial dislocation formation. Note that the range of Raman shifts is approximately 2 times as large in (d,e) than in (b,c).

these variations are meaningful at all, given the noise floor, they could arise from compositional variations in the alloy, growth inhomogeneities, roughness, and/or local delamination at the NM/substrate interface. The strain variations in these heterostructures (as shown for example in Figs. 2b and c) do not exhibit the typical crosshatch pattern indicative of dislocation pileup, as described below.

For comparison, maps of similar frequency shifts are shown in Figures 2d and e for a 20 nm $Si_{0.71}Ge_{0.29}$/12 nm Si/~2 μm $Si_{0.71}Ge_{0.29}$ heterostructure grown on a commercially available, polished, compositionally graded, and fully plastically relaxed $Si_{0.71}Ge_{0.29}$ substrate. The strain variations in this heterostructure follow the typical crosshatch pattern associated with strain relaxation via misfit dislocations in graded SiGe layers[11]. The strain inhomogeneities here arise from the non-uniform distribution of misfit dislocations that are relaxing the SiGe. The strain variations in the SiGe substrate translate to similar strain variations in the strained-Si QW. Similar shifts in the Raman frequencies of the Si-Si mode of the SiGe and the strained-Si layer indicate that the strained-Si layer is coherent with (i.e., strained to the alloy lattice constant of) the SiGe. The maximum variation in the Raman frequency shift in the heterostructures grown on the relaxed graded buffer layers is double ($\pm$0.8 cm^{-1}) that of the variation seen in the heterostructures grown on the NM substrates. These variations translate into a maximum strain variation of $\pm$0.10% in the strained-Si layer grown on the conventional substrate.

Mosaic tilt. In order to gain a better understanding of the crystalline quality of the strained-Si 2DEG, we measure the average mosaic tilt and variations in the local mosaic tilt in the heterostructures. We extract the area-averaged range of crystallographic orientations over the sample from x-ray diffraction reciprocal-space maps (RSMs) taken near the (224) reflection. The RSMs are collected with a laboratory x-ray diffractometer with a spot size of 1 mm × 1 cm using an asymmetric diffraction geometry. Figure 3 shows two such RSMs of similar heterostructures, one grown on a SiGe NM (Figure 3a) and the other grown on a commercially available polished, compositionally graded SiGe substrate (Figure 3b). Each heterostructure consists of a single SiGe layer with a composition matching the substrate and a thin Si QW. In both diffraction patterns, the x-ray reflection arising from the Si QW appears at the same in-plane wavevector as the SiGe reflection, indicating that the Si QW has the same in-plane lattice constant as SiGe.

The mosaic distribution of crystallographic orientations in the heterostructure is measured using the angular extent of the diffraction pattern of each layer. Mosaic tilt broadens the x-ray reflections along the reciprocal-space direction corresponding to the rotation of the sample, as indicated by the dashed line in Figure 3. The mosaic broadening has a full width at half-maximum of 0.05° in the SiGe layer grown on the SiGe NM, a factor of four smaller than the 0.2° broadening of the SiGe layer grown on the graded SiGe substrate. It is important to note that the large 0.2° mosaic spread of the SiGe layer on the compositionally graded substrate is typical of the best available such material. The larger value of mosaic spread arises from the plastic relaxation of SiGe during the creation of the compositionally graded substrate[11], a factor that is completely absent in the layers

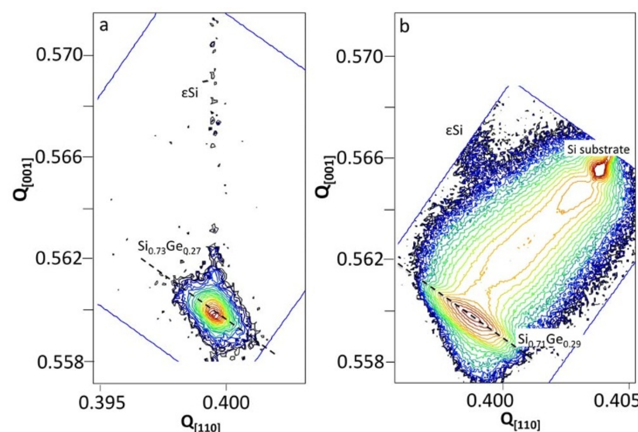

Figure 3 | Comparison of x-ray diffraction reciprocal-space maps (RSMs) for Si QW growth on SiGe NM and conventional compositionally graded SiGe substrates. (a) Growth on a SiGe NM substrate: 77 nm $Si_{0.73}Ge_{0.27}$/10 nm εSi/~1 μm $Si_{0.73}Ge_{0.27}$ grown on a 45 nm $Si_{0.73}Ge_{0.27}$ NM. (b) Growth on a compositionally graded SiGe substrate: 20 nm $Si_{0.71}Ge_{0.29}$/12 nm εSi/~2 μm $Si_{0.71}Ge_{0.29}$ grown on a polished $Si_{0.71}Ge_{0.29}$ substrate. The dashed line in both images is the constant-θ line; peak broadening along this line represents variations in crystalline tilt. The intensity in Figure 3b from the constant-composition peak to the Si substrate peak is from the graded region of the buffer layer. There is no substrate peak in the RSM of the heterostructure grown on the SiGe NM because the NM has a very different in-plane orientation (>10° in-plane twist from substrate) than the Si substrate it was transferred to. RSMs are taken around the off-axis (224) peak.

grown on SiGe NMs. The plastic relaxation of compositionally graded SiGe results from misfit dislocations and thus cannot be improved by modifying the composition profile during the Ge grading[11] or by other epitaxial growth techniques.

Figure 3 does not provide insight into the origin of the mosaic, because it shows averages over a large area. Synchrotron x-ray nanodiffraction allows the mapping of crystallographic orientation on a very small lateral scale. The distribution of local crystallographic orientations, obtained in this manner, in heterostructures grown on compositionally graded SiGe substrates[14,15] indicates that the mosaic blocks align with the crosshatch pattern created by the network of dislocations relaxing the SiGe. The maximum tilt variation observed in maps of large areas of more than 100 μm^2 is 0.2°, matching what is observed in area-averaged laboratory measurements[14]. The tilt is far less, only 0.02°, in smaller 25 μm^2 areas[15] because such maps fall within only one or a few mosaic blocks.

X-ray nanodiffraction maps of the magnitude and direction of the local crystalline tilt in a 10 × 10 μm^2 region of a strained-Si/SiGe heterostructure grown on a SiGe NM are shown in Figure 4. The sample is identical to the one for which the area-average diffraction pattern is shown in Figure 3a. The tilt was obtained from a map of diffraction patterns acquired near the (004) Bragg peak of the strained-Si QW using a procedure described in the Methods section. The maximum variation in the tilts shown in Figure 4 is 0.06°, matching the mosaic spread determined from the large-area average diffraction pattern in Figure 3a.

Because of a lack of crosshatch in these images, the microscopic mechanism leading to the tilting of the lattice in Si QWs grown on SiGe NMs is distinct from the dislocation-driven tilt observed in heterostructures grown on compositionally graded substrates. The tilt measured in heterostructures grown on NMs can arise from bending in the SiGe NM during or after it is transferred to the host substrate. The bending is small enough so that the NM strains elastically. SiGe NMs are very thin and flexible and thus conform to height variations arising from particulates, asperities, or steps at the bonded interface (Figure 4c). An epitaxial film grown on the transferred SiGe NM will have similar variations in its orientation. The bending of the SiGe NM does not have to be large to produce the tilts seen in this measurement. For example, a misorientation of 0.05° of the host Si surface produces terrace widths of 150 nm for single-atomic-step heights. A native oxide on the surface replicates the step structure. Similar height variations may also arise as a result of roughness introduced on the SiGe NM surface during transfer to a new host. The largest tilt variation in the map shown in Figure 4a is 0.05°, located in the feature at the bottom of the image. A 0.05° tilt over the width of this feature requires a step of only 1.3 nm at the interface between the SiGe NM and the host substrate. Wrinkles or bending of the SiGe NM of this magnitude would not be visible with an optical microscope.

If the SiGe NM is bending upon bonding to the new host, it is possible that this mechanism also accounts for the strain variations observed in the micro-Raman measurements (see Figures 2b and c). The strain will vary depending on the radius of curvature and/or the initial bonding points of the SiGe NM. Strain in the NM can result from bending alone. The SiGe NM conforms to the surface when transferred. If we extract a radius of curvature based on the tilt measured above (800–900 μm radius of curvature based on a 0.05° tilt over a 1.5 μm feature), we can use Stoney's equation to estimate the maximum strain at the top surface of the nanomembrane[20]. The maximum strain that could be induced for the measured crystalline tilt is consistent with the ±0.05% maximum deviation from the average strain seen in the Raman measurement in Figures 2b and c. The NM can also stretch as a result of capillary forces: if the NM is suspended over a valley, capillary forces can pull the NM into the valley, causing stretching and bending.

The above possibility for tilt variations in transferred NMs, although elegant, may be secondary to the effect of inhomogeneities and particles present at the host surface prior to NM transfer. In the above, the Si host is terminated with a chemical oxide and a wet NM transfer method is used[10], both procedures that are susceptible to contamination. It is expected that the magnitude of the surface roughness of the SiGe NM will be negligible compared to that of contaminants on the surface of the host substrate. Improved interfaces can be expected by transferring the SiGe NMs to H-terminated Si or using a dry-transfer method[21].

Conclusion

We have investigated local and global variations in strain and in crystalline tilt (mosaic) of strained-Si/relaxed SiGe heterostructures grown on elastically relaxed SiGe NM substrates. We have compared these, on macroscopic and microscopic length scales, to similar heterostructures grown on commercially available plastically relaxed compositionally graded SiGe substrates. NM-based heterostructures provided significantly better results: strain and tilt variations in these

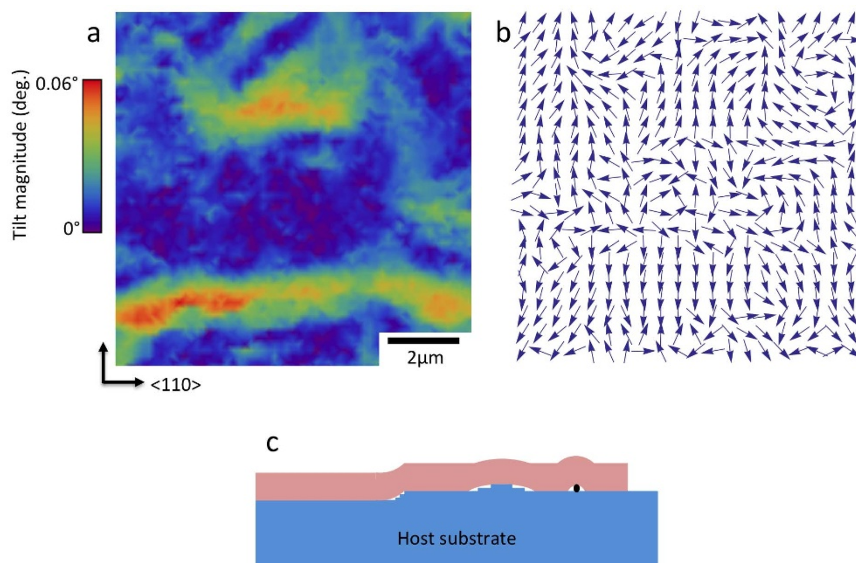

Figure 4 | Crystalline-tilt variation in a strained-Si QW layer grown on a SiGe NM transferred to an oxidized-Si host. (a) Areal plot of the crystalline-tilt magnitude in the strained-Si QW layer of a 77 nm $Si_{0.73}Ge_{0.27}$/10 nm εSi/~1 µm $Si_{0.73}Ge_{0.27}$ heterostructure grown on a 45 nm $Si_{0.73}Ge_{0.27}$ NM. (b) Directions from normal of the angular tilts shown in (a). (c) Schematic diagram of a possible mechanism leading to tilt in SiGe NM substrates. The SiGe NM can conform to surface roughness and particulates on the surface of the host substrate, causing the single-crystal NM to bend. Any heterostructure grown on top of the bent SiGe NM substrate will follow the tilt of the substrate.

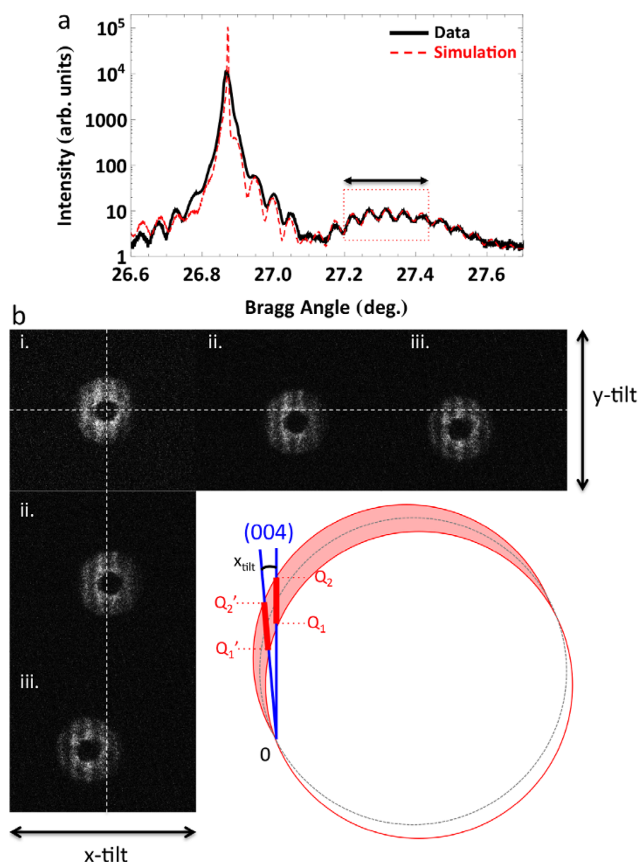

Figure 5 | Nanodiffraction data from a 77 nm $Si_{0.73}Ge_{0.27}$/10 nm εSi/~1 µm $Si_{0.73}Ge_{0.27}$ heterostructure grown on a 45 nm $Si_{0.73}Ge_{0.27}$ NM. (a) θ/2θ line scan around the (004) reflection at one spot (~1 µm). (b) Example data from tilt analysis (three points on the sample indicated by images i., ii., and iii.). The measured intensity on the CCD corresponds to the diffraction condition highlighted in the dashed box in (a). The y-tilt is proportional to the change in diffraction intensity in the y-direction on the CCD. The x-tilt is equal to the change in Bragg angle as measured directly by changes in the diffracted intensity along the x-direction of the CCD. Images ii. and iii. are aligned horizontally and vertically to image i. to show changes in the y-tilt and x-tilt, respectively. The diffracted intensity captured by the CCD is highlighted by the thick red line (between points Q_1 and Q_2) in the schematic diagram shown in (b). When the crystalline tilt of the sample changes in the diffraction plane, the diffraction condition changes (measured diffraction is now between Q_1' and Q_2').

heterostructures were considerably smaller than those in heterostructures grown on the graded SiGe and arise from different sources that likely can be eliminated. In contrast, the materials issues associated with compositional grading, which are conspicuously absent in the NM based heterostructures, cannot be eliminated. We expect to ameliorate or eliminate the remaining small tilt and strain variations in Si QWs grown on SiGe NM substrates by improving in particular the host surface and the transfer methodology. Crystalline semiconductor nanomembranes as growth substrates therefore represent a new paradigm that has the potential to enable many new technologies or enhance existing ones. For group IV semiconductor NMs, quantum electronics and quantum computation represents a particularly noteworthy area in which the materials improvements that NMs promise could significantly advance the field.

Methods

Raman microscopy. We measure the strain variation in the heterostructures with micro-Raman microscopy (LabRAM Aramis Horiba Jobin Yvon Confocal Raman Microscope). By using a laser wavelength of 442 nm (HeCd laser) we achieve significant surface sensitivity and are able to extract information from the heterostructure near the surface (volume that surrounds the Si QW); the penetration depth for 442 nm light in Si is ~300 nm and decreases with increasing Ge content[22]. The laser is focused with a 100× objective lens to a ~700 nm spot size and the measured points are spaced 300 nm apart. The frequencies of the Raman active modes from the strained-Si layer and the SiGe alloy (we use the Si-Si bond vibration) shift linearly as a function of biaxial strain[18,19]. A shift to lower frequency indicates an expansion in the in-plane lattice parameter for both materials. The frequency shifts are extracted by peak fitting and using a plasma peak from the laser (~283 cm^{-1}, calibrated to an unstrained bulk Si peak = 520.0 cm^{-1}) as a calibration for each spectrum. A weighted linear combination of symmetric Gaussian and Lorentzian line shapes is used to fit the strained-Si peak (80% Lorentzian, 20% Gaussian) and an asymmetric line shape is used to fit the Si-Si mode peak[23]. The stability of the instrument over the time scale of the 2D maps is ±0.3 cm^{-1}.

One area of Figures 2b and c illustrates the versatility of the micro-Raman measurements in analyzing differences in strain states between the strained-Si QW and the SiGe substrate. The strain variations in the strained-Si layer indicated by the arrows in Figure 2c do not appear to be random, as they are not in the surrounding regions of the SiGe (Figure 2b). The linear features are oriented along in-plane <110> crystallographic directions identical to the crosshatch pattern of plastically relaxed SiGe observed in Figure 2d. The pattern in Figure 2b thus indicates that the strained-Si layer is likely beginning to relax via misfit dislocations.

Nanodiffraction. The local crystalline tilt in the strained-Si QW is mapped with x-ray nanodiffraction at the Hard X-ray Nanoprobe of the Center for Nanoscale Materials located at sector 26-ID of the Advanced Photon Source at Argonne National Laboratory. We use x-rays with a photon energy of 10 keV focused with a Fresnel zone plate to a spot with an intensity FWHM of 50 nm on the sample. The focusing creates an angular divergence in the x-ray beam of 0.24°. The result is a simultaneous measurement through a small range of diffraction conditions at each point. The tilt is mapped by varying the position of the beam on the sample under a fixed x-ray incident angle. The x-ray focal spot is translated relative to the sample by the zone plate and sample using a combination of piezoelectric and motor-driven translation stages. The mosaic tilt is mapped by measuring changes in the specular diffraction pattern on a 2D detector near the (004) Bragg condition for the strained-Si QW layer. For more details on nanodiffraction please see[24].

Examples of the diffraction data collected on a two-dimensional charge coupled detector (CCD) are shown in Figure 5. Figure 5a is radial scan in reciprocal space (i.e., a conventional θ/2θ scan) acquired near the (004) reflection of the heterostructure. The three examples of 2D intensity plots taken at a single diffraction condition on different areas on the sample are shown in Figure 5b. The horizontal axis of the images corresponds to the angular direction on the detector parallel to the out-of-plane direction [001] direction in reciprocal space. A schematic diagram of the diffraction condition is shown in the inset of Figure 5b. The vertical direction of the diffraction images is perpendicular to the scattering plane. The annular distribution of intensity in Figure 5 arises from the distribution of intensity in the focused beam[24]. The vertical lines of intensity within the annular pattern in Figure 5 are thickness fringes of the heterostructure.

Horizontal sections through the images in Figure 5b correspond to diffraction line scans along the [001] direction of reciprocal space. A collection of horizontal profiles from data taken at different incident beam angles at the same position on the sample can thus be concatenated to form a complete scan along [001], identical to a conventional θ-2θ scan. The thicknesses of the SiGe capping layer and strained-Si QW layer and the strain in the Si QW can be extracted by fitting these scans with simulated diffraction patterns from model heterostructures.

The local mosaic tilt is extracted from variation in the location of the diffracted intensity in the diffraction images. Variations in crystalline tilt in the horizontal direction will result in changes in the diffraction condition, as illustrated in the inset of Figure 5b. Each pixel in the horizontal axis of the CCD corresponds to a different point in reciprocal space. The result is that the horizontal tilt, x_{tilt}, is equal to the change in the Bragg angle. The vertical tilt, y_{tilt}, is proportional to the change in position in diffracted intensity along the vertical axis of the diffraction image. The total magnitude of the crystallographic tilt is γ, given by $\cos(\gamma) = \cos(x_{tilt})*\cos(y_{tilt})$.

1. Sun, Y., Thompson, S. E. & Nishida, T. Physics of Strain Effects in Semiconductors and Metal-Oxide-Semiconductor Field-Effect Transistors. *J. Appl. Phys.* **101**, 104503 (2007).
2. Chu, M., Sun, Y., Aghoram, U. & Thompson, S. E. Strain: A Solution for Higher Carrier Mobility in Nanoscale MOSFETs. *Annu. Rev. Mater. Res.* **39**, 203–209 (2009).
3. Zhou, H. *et al.* Fast Flexible Electronics with Strained Silicon Nanomembranes. *Sci. Rep.* **3**, 1291 (2013).
4. Friesen, M. *et al.* Practical Design and Simulation of Silicon-Based Quantum-Dot Qubits. *Phys. Rev. B* **67**, 121301(R) (2003).
5. Sánchez-Pérez, J. R. *et al.* Direct-Bandgap Light-Emitting Germanium in Tensilely Strained Nanomembranes. *P. Natl. Acad. Sci. USA* **108**, 18893 (2011).
6. Schlom, D. G., Chen, L.-Q., Eom, C.-B., Rabe, K. M., Streiffer, S. K. & Triscone, J.-M. Strain Tuning of Ferroelectric Thin Films. *Annu. Rev. Mater. Res.* **37**, 589 (2007).
7. Haeni, J. H. *et al.* Room-Temperature Ferroelectricity in Strained $SrTiO_3$. *Nature* **430**, 758 (2004).
8. Goswami, S. *et al.* Controllable Valley Splitting in Silicon Quantum Devices. *Nat. Phys.* **3**, 41–45 (2007).
9. Kane, B. E. A Silicon-Based Nuclear Spin Quantum Computer. *Nature* **393**, 133–137 (1998).
10. Paskiewicz, D. M., Tanto, B., Savage, D. E. & Lagally, M. G. Defect-Free Single-Crystal SiGe: A New Material from Nanomembrane Strain Engineering. *ACS Nano* **5**, 5814–5822 (2011).
11. Mooney, P. M. Strain Relaxation and Dislocations in SiGe/Si Structures. *Mater. Sci. Eng.* **R17**, 105–146 (1996).
12. Sawano, K., Koh, S., Shiraki, Y., Usami, N. & Nakagawa, K. In-Plane Strain Fluctuation in Strained-Si/SiGe Heterostructures. *Appl. Phys. Lett.* **83**, 4339–4341 (2003).
13. Mermoux, M. *et al.* Strain in Epitaxial Si/SiGe Graded Buffer Structures Grown on Si(100), Si(110), and Si (111) Optically Evaluated by Polarized Raman Spectroscopy and Imaging. *J. Appl. Phys.* **107**, 013512 (2010).
14. Mooney, P. M., Jordan-Sweet, J. L., Noyan, I. C., Kaldor, S. K. & Wang, P.-C. Observation of Local Tilted Regions in Strained-Relaxed SiGe/Si Buffer Layers using X-ray Microdiffraction. *Appl. Phys. Lett.* **74**, 726 (1999).
15. Evans, P. G. *et al.* Nanoscale Distortions of Si Quantum Wells in Si/SiGe Quantum-Electronic Heterostructures. *Adv. Mater.* **24**, 5217–5221 (2012).
16. Scott, S. A. & Lagally, M. G. Elastically Strain-Sharing Nanomembranes: Flexible and Transferrable Strained Silicon and Silicon-Germanium Alloys. *J. Phys. D: Appl. Phys.* **40**, R75–R92 (2007).
17. Rogers, J. A., Lagally, M. G. & Nuzzo, R. G. Synthesis, Assembly and Applications of Semiconductor Nanomembranes. *Nature* **477**, 45–53 (2011).
18. Pezzoli, F. *et al.* Phonon Strain Shift Coefficients in $Si_{1-x}Ge_x$ Alloys. *J. Appl. Phys.* **103**, 093521 (2008).
19. Nakashima, S., Mitani, T., Ninomiya, M. & Matsumoto, K. Raman Investigation of Strain in Si/SiGe Heterostructures: Precise Determination of the Strain-Shift Coefficient of Si Bands. *J. Appl. Phys.* **99**, 053512 (2006).
20. Freund, L. B. & Suresh, S. Thin Film Materials: Stress, Defect Formation and Surface Evolution (Cambridge Univ. Press, Cambridge, 2003).
21. Kiefer, A. M., Paskiewicz, D. M., Clausen, A. M., Buchwald, W. R., Soref, R. A. & Lagally, M. G. Si/Ge Junctions Formed by Nanomembrane Bonding. *ACS Nano* **5**, 1179–1189 (2011).
22. De Wolf, I. Micro-Raman Spectroscopy to Study Local Mechanical Stress in Silicon Integrated Circuits. *Semicond. Sci. Technol.* **11**, 139–154 (1996).
23. Pezzoli, F. *et al.* Raman Spectroscopy of $Si_{1-x}Ge_x$ Epilayers. *Mater. Sci. Eng. B* **124–125**, 127–131 (2005).
24. Holt, M., Harder, R., Winarski, R. & Rose, V. Nanoscale Hard X-Ray Microscopy Methods for Materials Studies. *Annu. Rev. Mater. Res.* **43**, 3.1–3.29 (2013).

Acknowledgments

This research is funded by DOE, Grant No. DE-FG02-03ER46028. Facilities support by NSF, MRSEC program, is acknowledged. This work was performed, in part, at the Center for Nanoscale Materials, specifically the hard x-ray nanoprobe located at sector 26 of the Advanced Photon Source, a U. S. Department of Energy, Office of Science, Office of Basic Energy Sciences Users Facility under Contract No. DE-AC02-06CH11357. D.M.P. acknowledges support from the NSF Graduate Research Fellowship Program.

Author contributions

D.M.P., M.V.H. and P.G.E. developed the nanodiffraction methods and analyzed the synchrotron x-ray scattering results. D.M.P., D.E.S. and M.G.L. designed materials processing protocols. D.M.P. and D.E.S. fabricated materials. D.M.P., D.E.S., M.V.H., P.G.E. and M.G.L. acquired and analyzed data. D.M.P. and M.G.L. wrote the paper, with contributions from P.G.E. and M.V.H.

Additional information

Competing financial interests: D.M.P. and M.G.L. hold a patent for the underlying SiGe NM substrate fabrication technology and currently share in the royalties.

How to cite this article: Paskiewicz, D.M., Savage, D.E., Holt, M.V., Evans, P.G. & Lagally, M.G. Nanomembrane-based materials for Group IV semiconductor quantum electronics. *Sci. Rep.* **4**, 4218; DOI:10.1038/srep04218 (2014).

This work is licensed under a Creative Commons Attribution-NonCommercial-NoDerivs 3.0 Unported license. To view a copy of this license, visit http://creativecommons.org/licenses/by-nc-nd/3.0